European Journal of Organic Chemistry

EurJOC
European Journal of Organic Chemistry

Chemistry Europe
European Chemical Societies Publishing

RESEARCH ARTICLE

Succinct New Synthetic Route to Tetrathienoanthracene-Based Hole-Transporting Materials via Pd-Catalyzed Direct C—H/C—Br Coupling Reactions

Ling-Hui Lu[1] | Chu-Han Hsu[1] | Meng-De Wu[1] | Wei-Kai Chang[1] | Kun-Mu Lee[2,3] | Ming-Wei Hsu[1] | Ching-Yuan Liu[1]

[1]Department of Chemical and Materials Engineering, National Central University, Taoyuan City, Taiwan | [2]Department of Chemical and Materials Engineering & Center for Sustainability and Energy Technologies & Department of Pediatrics, Chang Gung Memorial Hospital, Chang Gung University, Taoyuan City, Taiwan | [3]College of Environment and Resources, Ming Chi University of Technology, New Taipei City, Taiwan

Correspondence: Kun-Mu Lee (kmlee@mail.cgu.edu.tw) | Ching-Yuan Liu (cyliu0312@ncu.edu.tw)

Received: 25 November 2025 | **Revised:** 21 December 2025 | **Accepted:** 29 December 2025

Keywords: direct C—H arylation | hole-transporting material | perovskite solar cell | synthesis design | tetrathienoanthracene

ABSTRACT

Tetrathienoanthracene (**TTA**) is a π-extended derivative of anthracene fused with four thiophene rings. **TTA** core-based small- and macromolecules have been extensively studied in the field of organic optoelectronic materials. However, by far, the existing synthetic routes to **TTA**-relevant molecules all relied on the traditional multistep synthesis involving tedious substrate prefunctionalization operations (10 steps). Herein, we reported a succinct new synthetic pathway (4 steps) to **TTA** core-based oligoarenes via palladium-catalyzed direct C—H/C—Br cross-couplings. Reaction conditions for the multifold direct C—H (hetero)arylations were optimized, thus allowing the smooth production of four new small molecules π-extended from the **TTA** core. These obtained oligoaryls were fabricated as hole-transport material in perovskite solar cells. Devices utilizing one of the **TTA**-based oligoaryls as hole-transport layer exhibited power conversion efficiencies up to 13.61%.

1 | Introduction

Anthracene is a readily available π-conjugated building block which has been extensively applied in the field of organic semiconducting materials because of its superior planarity, charge mobility, and molecular stability [1–7]. While four thiophene units were introduced onto anthracene by material scientists, a versatile new building block named tetrathienoanthracene (**TTA**) was created (Figure 1).

TTA exhibited numerous interesting optoelectronic characteristics and has also been widely employed as primary backbones of various π-conjugated oligomers and polymers for organic solar cells (OSCs) and organic field-effect transistors (OFETs). For instance, Komiyama and Yasuda synthesized a series of acceptor–donor–acceptor (A–D–A) type oligoaryls consisting of a **TTA** core for OSCs [8]. Perepichka's team reported two **TTA** core-based small molecules bearing alkyl chains, which displayed outstanding charge mobilities of corresponding OFET devices [9]. In 2011, Yu and coworkers disclosed the synthesis and OSC/OFET applications of a number of D–A type alternating copolymers using alkylated **TTA** as electron-donating monomer [10, 11]. More recently, Martin and Torres described, respectively, the preparation and fabrication of **TTA**-based oligomers as hole-transporting layer in perovskite solar cells (PSCs), showing promising power conversion efficiencies (PCEs) up to 18.76% [12, 13]. Except these two articles, no reports on the utilization of **TTA**-related molecules as hole-transporters for PSCs have appeared to date. Fabrication of a hole-transporting material (HTM) into perovskite-based solar cells has been a prerequisite to the enhancement of device performance and stability [14–17]. State-of-the-art hole-transporting materials for PSCs focused on the use of small-molecule HTMs since these π-conjugated oligo(hetero)aryls exhibited a number of advantages such as well-defined molecular weight, extensive synthetic diversity, and lower cost [18–24]. In addition to the most commonly used spiro-OMeTAD [25–29], PSCs incorporating several small-molecule

Ling-Hui Lu and Chu-Han Hsu contributed equally to this work.

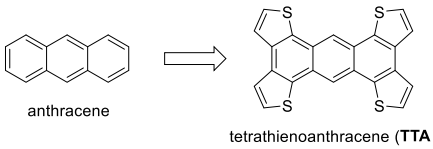

FIGURE 1 | Anthracene and its π-extended derivative fused with four thiophenes: tetrathienoanthracene (**TTA**).

HTMs like Trux-OMeTAD [30], donor–acceptor type molecules [31], benzotrithiophenes [32], or triphenylamine-carbazole hybrid oligomers [33, 34] also displayed impressive photovoltaic performances. Above HTMs-based PSCs showed comparable PCEs to the ones with spiro-OMeTAD. However, small-molecule HTMs incorporating a high-planarity core such as **TTA** is relatively less investigated. Moreover, although the highly fused aromatic derivatives like **TTA** are typically hard to synthesize, they might exhibit promising optoelectronic properties including the essential charge mobility [8–13]. Therefore, we wish to challenge the new design and synthesis of small-molecule HTMs with a high-planarity **TTA** core. Besides, we anticipated promoting the PCE of PSC devices employing **TTA** core-based oligoaryls as HTM. Up to date, material chemists continue searching for lower-cost while high-performance HTMs to keep up with spiro-OMeTAD.

In addition, we also noted that the equally important synthetic study on **TTA** and its π-extended oligoarenes still remained unexplored. In fact, the existing synthetic approaches to access **TTA** core-based molecules all relied on the use of Migita–Kosugi–Stille coupling and Suzuki reaction as key transformations, which required reactant prefunctionalizations including the generation and treatment of organotin and organoboron species. Nevertheless, as the pioneers, Fagnou [35], Ackermann [36], and Itami [37] groups disclosed numerous step-saving synthetic protocols based on direct C—H activation/arylations for novel π-conjugated organic materials. However, these succinct approaches are less focused on the facile preparation of multiply fused aromatic systems. Hence, as demonstrated in Scheme 1.

In contrast to the traditional multistep synthesis, herein we wish to report a succinct new synthetic route to tetrathienoanthracene and its π-extended oligoaryls via straightforward C—H/C—Br cross-coupling reactions, which could avoid tedious chemical transformations and considerably reduce the synthesis from

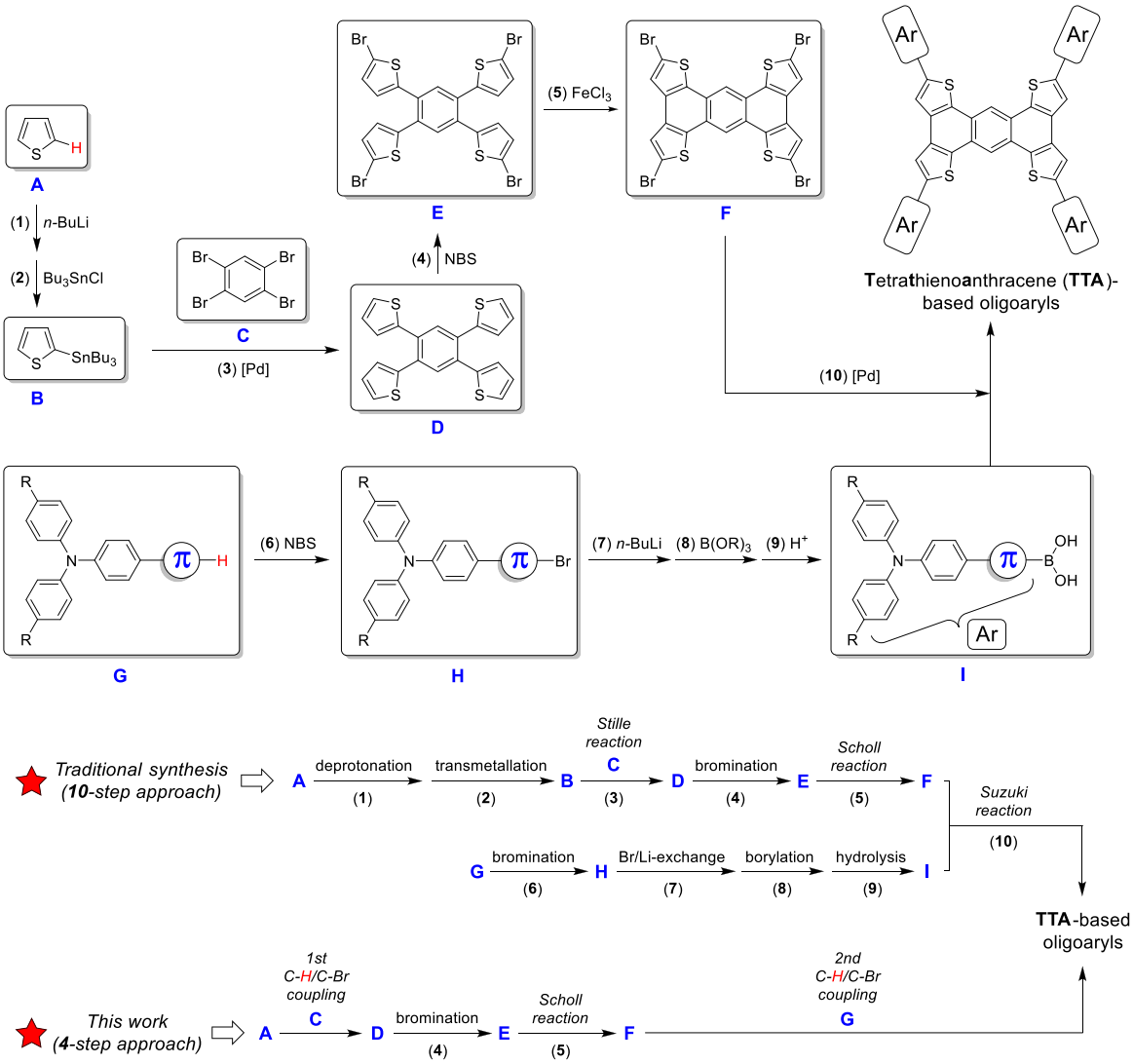

SCHEME 1 | Two synthetic pathways to access tetrathienoanthracene (**TTA**) core-based oligoaryls: 10- versus 4-step approach.

10- to 4-steps. In Scheme 1, comparably, while adopting a traditional synthetic plan, thiophene **A** was treated with *n*-BuLi (deprotonation) followed by the addition of Bu_3SnCl (transmetallation) to give a thienyltin reagent **B**. In the presence of a palladium-based catalyst, **B** proceeded Stille reaction with 1,2,4,5-tetrabromobenzene **C** to afford tetrathienylbenzene **D** that was then brominated by NBS to produce a tetrabromo-species **E**. Intramolecular oxidative coupling of **E** (Scholl reaction) was carried out by $FeCl_3$, generating tetrabromo-**TTA** (**F**). On the contrary, the end-group **G** required a series of chemical transformations (from step 6 to step 9) to form an arylboronic acid **I** that could undergo Suzuki coupling reaction with **F** under [Pd]-catalysis to reach the targeted tetrathienoanthracene (**TTA**) core-based oligoaryls. Abovementioned was a general synthetic pathway frequently used in literatures to access **TTA** and its related molecules [12, 13].

2 | Results and Discussion

In this work, we proposed a 4-step synthesis shortcut, in which Stille and Suzuki reactions were skipped. Instead, the C—H arylation of thiophene **A** was conducted directly with **C** (first C—H/C—Br cross-coupling), thus facilely leading to obtain a tetrathienylbenzene **D**. Similar to the reported synthesis discussed in Scheme 1, bromination and Scholl reaction were sequentially performed, which converted **D** through **E** to the key building block **F**. Finally, tetrabromo-**TTA** (**F**) directly underwent the second C—H/C—Br coupling reaction with the unprefunctionalized end-group **G** to afford identical targets (**TTA**-based oligomers). Therefore, we have omitted steps 1–3 and steps 6–10 for the preparation of essential thienyltin and arylboronic acids required in traditional synthetic pathways. To the best of our knowledge, this step-saving synthetic approach represents an unprecedented example to access the **TTA** derivative **F** and its π-extended oligomers.

To access the targeted molecules smoothly, part of the reaction parameters for the 1st C—H/C—Br cross-coupling were optimized by the treatment of thiophene **A** with 1,2,4,5-tetrabromobenzene **C** under a [Pd]-based catalysis. Relevant results were collected and summarized in Table 1. Initially, the reaction was conducted with a commonly used C—H arylation condition: $Pd(OAc)_2$/PPh_3/PivOH/K_2CO_3/DMAc, according to one of our [38] previously reported and other related pioneering publications [39–51]. However, we observed a significant amount of unreacted **C**, thus a fairly poor isolated yield of desired **D** was obtained (9%, entry1). We tried to reduce the addition of solvent (0.5 mL) so that the coupling proceeded under a more concentrated condition. This did not make any obvious improvement (11%, entry 2). We then decided to employ reactant **A** (thiophene) as solvent to replace DMAc. Besides, reaction time was extended from 24 to 48 h. In these two experiments, slightly improved isolated yields of **D** were observed (22%, 26%; entries 3, 4). Comparably, it was found the reaction could take place even without the use of PivOH (27%, entry 5). Hence, based on the result of entry 5, a variety of ligands were screened in the following entries. P(*o*-, or *m*-tolyl)$_3$ gave poor conversions (15%, 17%; entries 6, 7). Tri(alkyl)phosphine ligands such as P(*t*-Bu)$_3$ was not effective at all (trace, entry 8), whereas P(Cy)$_3$ and P(adamantly)$_2$(*n*-Bu) demonstrated relatively better yields (34%, 22%; entries 9, 10). SPhos, a dialkylaryl-substituted phosphine, led to the formation of **D** in 21% (entry 11). Depending on the above results, we supposed that, up to this point, P(Cy)$_3$ would be the best ligand for the direct C—H monoarylation of thiophene. Meanwhile, we wondered if the present reaction could be switched back to 24 h. Therefore, in entry 12, C—H/C—Br cross-coupling was performed with $Pd(OAc)_2$/P(Cy)$_3$/K_2CO_3 in thiophene at 145°C for 24 h. We were pleased to learn that shortening the reaction time did not greatly alter the reaction outcome (33%, entry 12), compared to the result provided in entry 9 (34%). This inspired us to continue screening other types of ligands. The bidentate ones including dppe, dppp, and dppf were also examined, which generated the desired product in poor yields (11%–15%, entries 13–15). A number of *N*,*N*′-type ligands (L11 ~ L14) were then investigated. It was worth noting that 2,2′-bipyridyl displayed a relatively promising reaction conversion (35%, entry 16), while others exhibited an inefficient catalytic ability with $Pd(OAc)_2$, thus giving targeted **D** all in trace amount (entries 17–19). Finally, based on the consideration of the result acquired in entry 16, we performed the coupling reaction again with the regular conditions provided in footnote [a] of Table 1 (the quantity of 2,2′-bipyridyl was increased to 30 mol%). The result revealed a notable improvement on isolated yield of **D** (62%, entry 20).

Next, as shown in Scheme 2 describing our 4-step synthetic route to **TTA** core-based oligoaryls, the optimum reaction conditions for step 1 (entry 20 of Table 1) were successfully utilized to produce compound **D** in moderate yield (62%). Bromination of **D** with NBS afforded 1,2,4,5-tetrakis(5-bromothiophen-2-yl)benzene **E** in 68% yield. **E** underwent an intramolecular dehydrogenative homocoupling reaction (Scholl reaction) mediated by $FeCl_3$, which generated a cyclized adduct **F** in good isolated yield (80%). Subsequently, four different end-group molecules (**G1~4**) bearing 3,4-ethylenedioxythiophene (EDOT) or ethyne moiety as π-spacers were individually introduced to the core molecule **F** (**TTA**) either by 2nd C—H/C—Br cross-couplings or Sonogashira reactions. This led to form four oligoarenes for the potential applications as HTMs: **WKC04** (55%), **WKC05** (43%), **LHL01** (83%), and **LHL04** (90%). Reaction conditions and procedures for the above discussions were detailed in Supporting Information.

UV–vis absorption, electrochemical properties, thermal stability, and hole-mobilities of the obtained HTM molecules were investigated and relevant data were collected in Table 2. It was found that **TTA**-based oligoaryls consisting of electron-abundant π-spacers (EDOT) exhibited narrower optical bandgaps (ΔE_g^{opt} = 2.36–2.38 eV for **WKC04** and **WKC05**), whereas **LHL01**&**04** with ethynes displayed wider ΔE_g^{opt} of 2.50 and 2.53 eV. Cyclic voltammetry experiments were conducted and the results indicated that **WKC04**&**05** incorporating EDOT moieties possessed the lowest-lying highest occupied molecular orbital (HOMO, E_{HOMO} = −5.66 eV, −5.69 eV). In addition, **LHL04** also showed a relatively lower-lying HOMO energy level of −5.56 eV. Their E_{HOMO} were even lower-lying than that of the perovskite layer (PVSK, E_{HOMO} = −5.50 eV), thus implying **WKC04**&**05** and **LHL04** may not efficiently extract holes from PVSK. Further, the thermal stability of each HTM was assessed by performing thermal gravimetric analysis. Except **WKC04**, other oligoaryls exhibited moderate thermal stabilities (decomposition temperature > 300°C, T_d = 310–338°C). In addition, hole-mobility (μ_h) of the HTMs was evaluated by measuring their current density–voltage in the region of space-charge limited

TABLE 1 | Reaction condition optimizations of the 1st C—H/C—Br coupling.[acd]

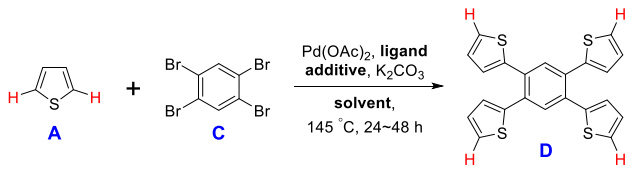

Entry	Ligand	Additive	Solvent	Time (h)	Yield (%)[f]
1	L1	PivOH	DMAc	24	9
2[b]	L1	PivOH	DMAc	24	11
3	L1	PivOH	Th	24	22
4	L1	PivOH	Th	48	26
5	L1	—	Th	48	27
6	L2	—	Th	48	15
7	L3	—	Th	48	17
8	L4	—	Th	48	trace
9	L5	—	Th	48	34
10	L6	—	Th	48	22
11	L7	—	Th	48	21
12	L5	—	Th	24	33
13	L8	—	Th	24	15
14	L9	—	Th	24	14
15	L10	—	Th	24	11
16	L11	—	Th	24	35
17	L12	—	Th	24	trace
18	L13	—	Th	24	trace
19	L14	—	Th	24	trace
20[e]	**L11**	**—**	**Th**	**24**	**62**

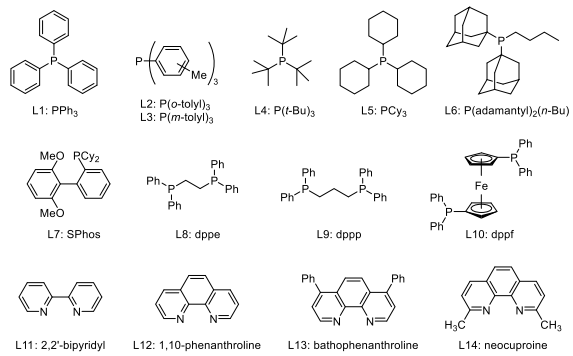

[a]Unless specified, the C—H/C—Br coupling reactions were conducted with 1,2,4,5-tetrabromobenzene **C** (1.00 mmol) and thiophene **A** (20 mmol) in the presence of $Pd(OAc)_2$ (15 mol%, 0.15 mmol), ligand (30 mol%, 0.30 mmol), PivOH (60 mol%, 0.60 mmol), and K_2CO_3 (4.00 mmol) in DMAc (1.0 mL) at 145°C under N_2 for 24–48 h.
[b]DMAc was reduced to 0.5 mL.
[c]From entry 3 through 20, thiophene (Th) was used as reaction solvent (3.0 mL).
[d]From entry 13 through 19, the quantity of each bidentate ligand was reduced (15 mol%, 0.15 mmol).
[e]Addition of the bipyridyl was increased to a regular quantity (30 mol%, 0.30 mmol), as described in footnote [a].
[f]Isolated yields.

current. The data revealed that **LHL01**/**04** possessed relatively lower hole-mobilities of $1.69\text{x}10^{-4} \sim 2.49 \times 10^{-4}$ $cm^2V^{-1}s^{-1}$ while compare to **spiro-OMeTAD** ($\mu_h = 2.97 \times 10^{-4}$ $cm^2V^{-1}s^{-1}$). The μ_h of **WKC04**&**05** is negligible (≈0), which also suggested they are unable to perform as effective HTMs. Synthesized oligoaryls were individually fabricated as hole-transport layer in corresponding PSCs. Their photovoltaic performance was evaluated and relevant parameters were summarized in Table 3. In general,

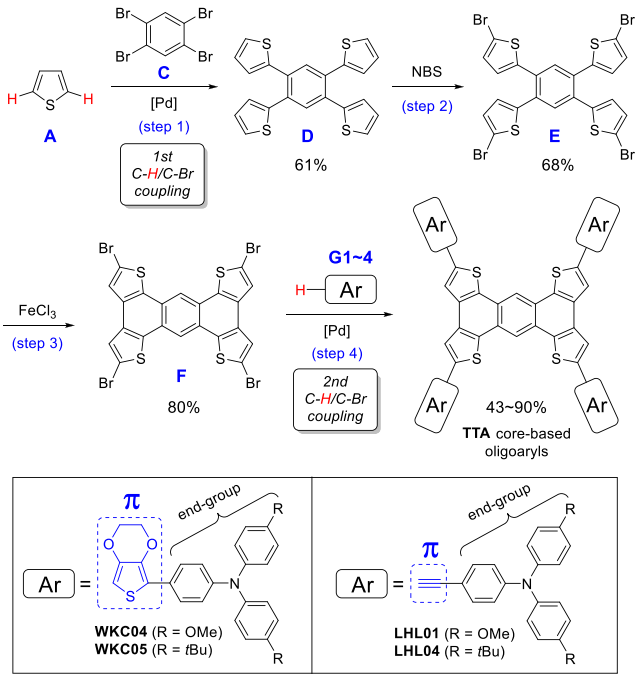

SCHEME 2 | Facile preparation of various **TTA** core-based oligoaryls by our 4-step synthetic approach.

to a solution of each HTM molecule in chlorobenzene was added lithium bis(trifluoromethane)sulfonimide (Li-TFSI) and 4-*t*-butylpyridine (*t*BP) as doping agents prior to spin-coatings (procedures for device fabrications were detailed in the Supporting Information). Devices using **WKC04** as HTM were found unstable under solar irradiation; thus, the photovoltaic parameters could not be obtained. Similarly, PSCs with **WKC05** exhibited a poor PCE of 0.52%. We speculated that **WKC04**&**05** bearing EDOT groups were unable to act as effective HTMs due to their unsuitable E_{HOMO} for hole-extractions, as discussed in the last section (Table 2). Next, **LHL01**-based PSCs displayed the best PCE up to 13.61%, whereas **LHL04**-based devices showed an awful PCE of 0.48%, presumably also owing to its relatively lower-lying E_{HOMO} of −5.56 eV, which led to an inefficient hole-extraction from the PVSK layer.

The PCE of some PSCs is approaching zero (**WKC04**-, **WKC05**-, or **LHL04**-based PSC devices). We supposed the poor performance might not arise from the alignment between the conduction band of perovskite layer and these HTMs. Instead, it may result from the mismatch between the valence band of perovskite layer and the HOMO level of these HTMs. As shown in Figure 2, the perovskite layer exhibits a valence band of −5.50 eV. However, the HOMO level of **WKC04**, **WKC05**, and **LHL04** is significantly lower-lying than that of perovskite layer, which introduces an energetic barrier for hole-extraction. When the HOMO of HTM is relatively lower-lying than the valence band of PVK, holes cannot be efficiently extracted from the PVK to the HTM, thus leading to a considerable charge recombination and resulting in near-zero device efficiency.

In addition, the photovoltaic performance of the PSC devices with each HTM (doped and undoped) was demonstrated by the diagram of photocurrent density–voltage (*J*-*V*), as provided in Figure 3. It was found that, except the devices with **LHL01**,

TABLE 2 | The optical, electrochemical, thermal properties, and the hole mobility of **WKC04**, **WKC05**, **LHL01**, and **LHL04**.

HTMs	ΔE_g^{opt} (eV)[a]	E_{HOMO} (eV)[b]	E_{LUMO} (eV)[c]	T_d (°C)[d]	Hole mobility ($cm^2\ V^{-1}\ s^{-1}$)
WKC04	2.38	−5.66	−3.28	283	—
WKC05	2.36	−5.69	−3.33	338	—
LHL01	2.50	−5.40	−2.90	337	2.49×10^{-4}
LHL04	2.53	−5.56	−3.03	310	1.69×10^{-4}

[a]UV–vis absorption spectra were measured in dichloromethane solution. ΔE_g^{opt} was calculated from the absorption onset of UV–Vis spectra. $\Delta E_g^{opt} = 1240/\lambda_{onset}$.
[b]$E_{HOMO} = -(E_{ox,\ onset(vs.Fc/Fc^+)} + 5.16)$ eV.
[c]$E_{LUMO} = E_{HOMO} + \Delta E_g^{opt}$.
[d]T_d was obtained at 5% weight loss of each **TTA**-based oligomers.

TABLE 3 | Photovoltaic capabilities of the perovskite solar cells using **WKC04**, **WKC05**, **LHL01**, or **LHL04** as HTMs.[ab]

HTMs		V_{oc} (V)	J_{sc} ($mAcm^{-2}$)	FF (%)	PCE (%)
WKC04		—	—	—	—
WKC05	Best	0.79	1.29	51.06	0.52
	average	0.64 ± 0.12	1.40 ± 0.21	51.71 ± 2.17	0.45 ± 0.04
LHL01	Best	1.04	17.63	74.13	13.61
	average	1.03 ± 0.01	15.33 ± 1.28	74.69 ± 3.14	11.79 ± 0.87
LHL04	Best	0.88	1.73	31.35	0.48
	average	0.71 ± 0.23	1.74 ± 0.46	30.64 ± 2.36	0.36 ± 0.12
spiro-OMeTAD	Best	1.06	23.05	75.84	18.59
	average	1.02 ± 0.03	23.38 ± 0.67	74.22 ± 1.57	17.78 ± 0.62

[a]Each HTM layer of corresponding PSC devices was added two doping agents: 4-*t*-butylpyridine and Li-TFSI. The statistical data were calculated based on 6–8 cells.
[b]Reverse scans.

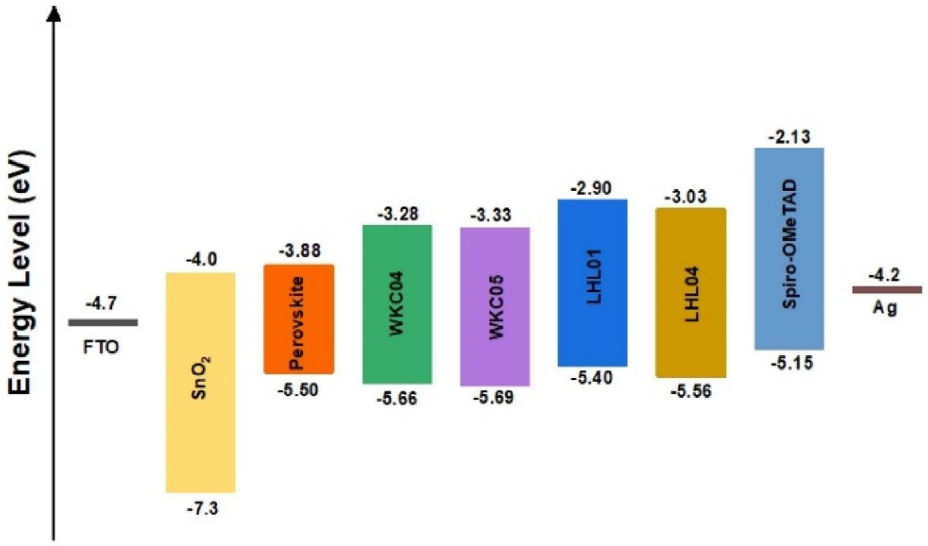

FIGURE 2 | The energy level diagram of each component of a perovskite solar cell.

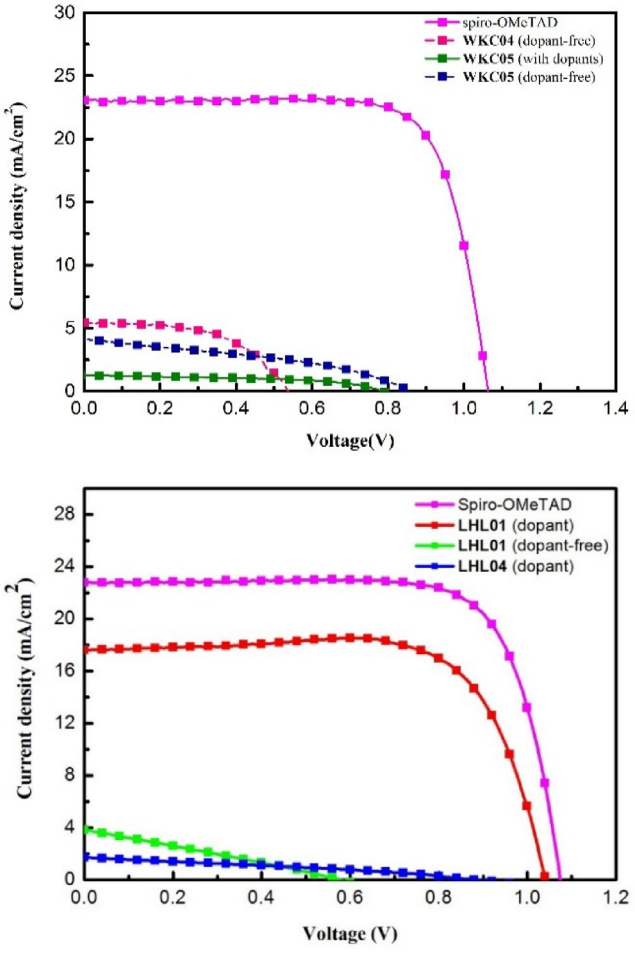

FIGURE 3 | Photocurrent density–voltage (*J-V*) curves of perovskite solar cells using **WKC04**, **WKC05**, **LHL01**, or **LHL04** as hole-transporting layer.

other PSCs gave poor or negligible *J-V* values under dopant-free conditions.

In order to further investigate the hole-extraction ability of each HTM, devices with the configuration of glass/perovskite/HTM (**LHL01** and **LHL04**) were individually fabricated for the measurement of steady-state photoluminescence (PL) and time-resolved PL. Relevant spectra were provided in Supporting Information (Figures S5 and S6). In general, devices with the HTM bearing OMe substituents (**LHL01**) demonstrated relatively stronger PL quenching effect, indicating that **LHL01** are able to extract holes more efficiently at the interface between the perovskite layer and the corresponding hole-transport layer.

Furthermore, as summarized in Table 4, we compared the production costs of our four-step synthetic route to **LHL01** with those reported in the literature. The previously reported approach involved a ten-step synthesis, resulting in a higher overall cost of approximately USD 43.94 for generating 1.00 g of **TTA3** [13]. In contrast, our synthetic strategy required only four chemical transformations, leading to a lower estimated production cost of USD 39.97 per 1.00 g of **LHL01**. The reduced number of synthetic steps decreased materials consumption, purification demand, and operational complexity. This comparison highlights the practical and economic advantages of the present synthetic shortcut. The corresponding flow chart and detailed cost tables were provided in Supporting Information. The cost assessment was conducted based on the model reported by Osedach [52].

Finally, to enable a direct comparison between our synthetic route and the previously reported method, we evaluated the E-factors of both approaches. The E-factor analysis included all sources of chemical waste, encompassing excess reagents, aqueous and organic solvents, and silica gel used for purification.

TABLE 4 | Comparison regarding the cost-analysis for the reported TTA3 and our synthesized **LHL01**.

HTMs	Synthetic step	Cost[a] (USD)
TTA3 (literature [13])	10 steps	43.94
LHL01 (this work)	4 steps	39.97

[a]The cost was estimated based on taking into consideration of all required reagents, chemicals, and solvents employed in each synthesis and purification step for the production of 1.00 mmol of **TTA3** and **LHL01**.

Our four-step synthesis of **LHL01** exhibited an overall E-factor of 1867.43, whereas the reported ten-step route to **TTA3** showed a substantially higher E-factor of 2915.2. The lower E-factor obtained from our method indicated a significant reduction in waste generation per unit mass of the final isolated product. Overall, this comparison demonstrated that our synthetic route is more efficient and environmentally favorable than the previously reported synthesis. E-factor calculations were detailed in the Supporting Information.

3 | Conclusion

We have successfully developed a step-saving new synthetic route to a series of **TTA** core-based oligoarenes through straightforward C—H/C—Br coupling reactions. This synthetic pathway represented a viable alternative to the reported syntheses requiring additional substrate prefunctionalization steps prior to Suzuki and Stille reactions. Besides, this work also demonstrated the screening of reaction conditions for the first C—H/C—Br cross-coupling in order to acquire the optimum reaction parameters. Hence, six π-extended oligomers including **WKC04**, **WKC05**, **LHL01**, and **LHL04** were facilely obtained in moderate to good isolated yields. These molecules were fabricated as hole-transporting materials in perovskite-based solar cells, one of which displaying 13.61% PCE (PSC devices with **LHL01**). Development of succinct synthetic routes for π-conjugated organic materials is currently underway in our laboratory.

4 | Experimental Section

General procedure for the synthesis of compound D: to a solution of $Pd(OAc)_2$ (34 mg, 0.15 mmol), 2,2′-bipyridyl (46 mg, 0.30 mmol), and K_2CO_3 (552 mg, 4.00 mmol) in thiophene (3 mL) in a sealed tube was added 1,2,4,5-tetrabromobenzene C (1.00 mmol) under N_2. The reaction mixture was then heated at 145°C under N_2 for 24 h. After the reaction mixture had cooled to room temperature, water (10 mL) was added. The mixture was extracted with dichloromethane (2 × 20 mL), and the combined organic layers were washed with brine (50 mL), dried (Na_2SO_4), and concentrated in vacuo. Purification by flash chromatography (dichloromethane : hexanes = 10 : 90) afforded the desired product D (252 mg, 62%, pale yellow solid)

Acknowledgments

Financial support provided by National Science and Technology Council (NSTC), Taiwan (NSTC 113-2113-M-008−004 and 111-2223-E-182-001-MY4), National Central University (NCU), Chang Gung University (URRPD2N0011), and Chang Gung Memorial Hospital, Linkou, Taiwan (CMRPD2M0042) is gratefully acknowledged. The authors also thank the instrument center located at R&D office of NCU for the technical support of NMR and mass analysis.

Funding

National Science and Technology Council (NSTC 113-2113-M-008-004; 111-2223-E-182-001-MY4).

Conflicts of Interest

The authors declare no conflicts of interest.

References

1. J. Huang, J.-H. Su, and H. Tian, "The Development of Anthracene Derivatives for Organic Light-Emitting Diodes," *Journal of Materials Chemistry* 22 (2012): 10977.

2. M. Zhu, T. Ye, C.-G. Li, et al., "Efficient Solution-Processed Nondoped Deep-Blue Organic Light-Emitting Diodes Based on Fluorene-Bridged Anthracene Derivatives Appended with Charge Transport Moieties," *The Journal of Physical Chemistry C* 115 (2011): 17965.

3. A. Marrocchi, F. Silvestri, M. Seri, A. Facchetti, A. Taticchi, and T. J. Marks, "Conjugated Anthracene Derivatives as Donor Materials for Bulk Heterojunction Solar Cells: Olefinic versus Acetylenic Spacers," *Chemical Communications* 11 (2009): 1380.

4. H. Meng, F. Sun, M. B. Goldfinger, et al., "2,6-Bis[2-(4-Pentylphenyl) Vinyl]Anthracene: A Stable and High Charge Mobility Organic Semiconductor with Densely Packed Crystal Structure," *Journal of the American Chemical Society* 128 (2006): 9304.

5. D. J. Gundlach, J. A. Nichols, L. Zhou, and T. N. Jackson, "Thin-film Transistors based on Well-ordered Thermally Evaporated Naphthacene Films," *Applied Physics Letters* 80 (2002): 2925.

6. C. Teng, X. Yang, C. Yang, et al., "Molecular Design of Anthracene-Bridged Metal-Free Organic Dyes for Efficient Dye-Sensitized Solar Cells," *The Journal of Physical Chemistry C* 114 (2010): 9101.

7. X. Liu, F. Kong, R. Ghadari, et al., "Anthracene–Arylamine Hole Transporting Materials for Perovskite Solar Cells," *Chemical Communications* 53 (2017): 9558.

8. H. Komiyama, C. Adachi, and T. Yasuda, "Star-Shaped and Linear π-Conjugated Oligomers Consisting of a Tetrathienoanthracene Core and Multiple Diketopyrrolopyrrole Arms for Organic Solar Cells," *Beilstein Journal of Organic Chemistry* 12 (2016): 1459.

9. J. L. Brusso, O. D. Hirst, A. Dadvand, et al., "Two-Dimensional Structural Motif in Thienoacene Semiconductors: Synthesis, Structure, and Properties of Tetrathienoanthracene Isomers," *Chemistry of Materials : A Publication of the American Chemical Society* 20 (2008): 2484.

10. F. He, W. Wang, W. Chen, et al., "Tetrathienoanthracene-Based Copolymers for Efficient Solar Cells," *Journal of the American Chemical Society* 133 (2011): 3284.

11. C. Li, N. Zheng, H. Chen, et al., "Synthesis, Characterization, and Field-Effect Transistor Properties of Tetrathienoanthracene-Based Copolymers Using a Two-Dimensional π-Conjugation Extension Strategy: A Potential Building Block for High-Mobility Polymer Semiconductors," *Polymer Chemistry* 6 (2015): 5393.

12. I. Zimmermann, J. Urieta-Mora, P. Gratia, et al., "High-Efficiency Perovskite Solar Cells Using Molecularly Engineered, Thiophene-Rich, Hole-Transporting Materials: Influence of Alkyl Chain Length on Power Conversion Efficiency," *Advanced Energy Materials* 7 (2016): 1601674.

13. D. E. M. Rojas, K. T. Cho, Y. Zhang, et al., "Tetrathienoanthracene and Tetrathienylbenzene Derivatives as Hole-Transporting Materials for Perovskite Solar Cell," *Advanced Energy Materials* 8 (2018): 1800681.

14. S. Ameen, M. A. Rub, S. A. Kosa, et al., "Perovskite Solar Cells: Influence of Hole Transporting Materials on Power Conversion Efficiency," *ChemSusChem* 9 (2016): 10.

15. Z. Yu and L. Sun, "Recent Progress on Hole-Transporting Materials for Emerging Organometal Halide Perovskite Solar Cells," *Advanced Energy Materials* 5 (2015): 1500213.

16. L. Calió, S. Kazim, M. Grätzel, and S. Ahmad, "Hole-Transport Materials for Perovskite Solar Cells," *Angewandte Chemie International Edition* 55 (2016): 14522.

17. J. U. Mora, I. G. Benito, A. M. Ontoria, and N. Martín, "Hole Transporting Materials for Perovskite Solar Cells: A Chemical Approach," *Chemical Society Reviews* 47 (2018): 8541.

18. C. R. Seco, L. Cabau, A. V. Ferran, and E. Palomares, "Advances in the Synthesis of Small Molecules as Hole Transport Materials for Lead Halide Perovskite Solar Cells," *Accounts of Chemical Research* 51 (2018): 869.

19. H. Li, K. Fu, A. Hagfeldt, M. Grätzel, S. G. Mhaisalkar, and A. C. Grimsdale, "A Simple 3,4-Ethylenedioxythiophene Based Hole-Transporting Material for Perovskite Solar Cells," *Angewandte Chemie International Edition* 53 (2014): 4085.

20. K. Rakstys, A. Abate, M. L. Dar, et al., "Triazatruxene-Based Hole Transporting Materials for Highly Efficient Perovskite Solar Cells," *Journal of the American Chemical Society* 137 (2015): 16172.

21. H. Nishimura, N. Ishida, A. Shimazaki, et al., "Transporting Materials with a Two-Dimensionally Expanded π-System around an Azulene Core for Efficient Perovskite Solar Cells," *Journal of the American Chemical Society* 137 (2015): 15656.

22. M. Saliba, S. Orlandi, T. Matsui, et al., "A Molecularly Engineered Hole-Transporting Material for Efficient Perovskite Solar Cells," *Nature Energy* 1 (2016): 15017.

23. C. Lu, I. T. Choi, J. Kim, and H. K. Kim, "Simple Synthesis and Molecular Engineering of Low-Cost and Star-Shaped Carbazole-Based Hole Transporting Materials for Highly Efficient Perovskite Solar Cells," *Journal of Materials Chemistry A* 5 (2017): 20263.

24. M. S. Kang, S. D. Sung, I. T. Choi, et al., "Novel Carbazole-Based Hole-Transporting Materials with Star-Shaped Chemical Structures for Perovskite-Sensitized Solar Cells," *ACS Applied Materials & Interfaces* 7 (2015): 22213.

25. H. Zhou, Q. Chen, G. Li, et al., "Interface Engineering of Highly Efficient Perovskite Solar Cells," *Science* 345 (2014): 542.

26. N. Ahn, D. Y. Son, I. H. Jang, S. M. Kang, M. Choi, and N. G. Park, "Highly Reproducible Perovskite Solar Cells with Average Efficiency of 18.3% and Best Efficiency of 19.7% Fabricated via Lewis Base Adduct of Lead(II) Iodide," *Journal of the American Chemical Society* 137 (2015): 8696.

27. M. Liu, M. B. Johnston, and H. J. Snaith, "Efficient Planar Heterojunction Perovskite Solar Cells by Vapour Deposition," *Nature* 501 (2013): 395.

28. U. Bach, Y. Tachibana, J. E. Moser, et al., "Charge Separation in Solid-State Dye-Sensitized Heterojunction Solar Cells," *Journal of the American Chemical Society* 121 (1999): 7445.

29. U. Bach, D. Lupo, P. Comte, et al., "Solid-State Dye-Sensitized Mesoporous TiO_2 Solar Cells with High Photon-to-Electron Conversion Efficiencies," *Nature* 395 (1998): 583.

30. C. Huang, W. Fu, C.-Z. Li, et al., "Dopant-Free Hole-Transporting Material with a C 3 h Symmetrical Truxene Core for Highly Efficient Perovskite Solar Cells," *Journal of the American Chemical Society* 138 (2016): 2528.

31. Z. Li, Z. Zhu, C.-C. Chueh, et al., "Rational Design of Dipolar Chromophore as an Efficient Dopant-Free Hole-Transporting Material for Perovskite Solar Cells," *Journal of the American Chemical Society* 138 (2016): 11833.

32. A. M. Ontoria, I. Zimmermann, I. G. Benito, et al., "Benzotrithiophene-Based Hole-Transporting Materials for 18.2% Perovskite Solar Cells," *Angewandte Chemie International Edition* 55 (2016): 6270.

33. P. Gratia, A. Magomedov, T. Malinauskas, et al., "A Methoxydiphenylamine-Substituted Carbazole Twin Derivative: An Efficient Hole-Transporting Material for Perovskite Solar Cells," *Angewandte Chemie International Edition* 54 (2015): 11409.

34. S. J. Park, S. Jeon, I. K. Lee, et al., "Inverted Planar Perovskite Solar Cells with Dopant-Free Hole Transporting Material: Lewis Base-Assisted Passivation and Reduced Charge Recombination," *Journal of Materials Chemistry A* 5 (2017): 13220.

35. D. J. Schipper and K. Fagnou, "Direct Arylation as a Synthetic Tool for the Synthesis of Thiophene-Based Organic Electronic Materials," *Chemistry of Materials : A Publication of the American Chemical Society* 23 (2011): 1594.

36. L. Ackermann, R. Vicente, and A. R. Kapdi, "Transition-Metal-Catalyzed Direct Arylation of (Hetero)Arenes by C(**t**)H Bond Cleavage," *Angewandte Chemie International Edition* 48 (2009): 9792.

37. I. A. Stepek and K. Itami, "Recent Advances in C–H Activation for the Synthesis of π-Extended Materials," *ACS Materials Letters* 2 (2020): 951.

38. T.-J. Lu, P.-H. Lin, K.-M. Lee, and C.-Y. Liu, "End-Capping Groups for Small-Molecule Organic Semiconducting Materials: Synthetic Investigation and Photovoltaic Applications through Direct C–H (Hetero)arylation," *European Journal of Organic Chemistry* (2017): 111.

39. B. Liégault, D. Lapointe, L. Caron, A. Vlassova, and K. Fagnou, "Establishment of Broadly Applicable Reaction Conditions for the Palladium-Catalyzed Direct Arylation of Heteroatom-Containing Aromatic Compounds," *The Journal of Organic Chemistry* 74 (2009): 1826.

40. R. L. Carvalho, E. B. T. Diogo, S. L. Homölle, S. Dana, E. N. S. Júnior, and L. Ackermann, "The Crucial Role of Silver(I) Salts as Additives in C–H Activation Reactions: Overall Analysis of Their Versatility and Applicability," *Chemical Society Reviews* 52 (2023): 6359.

41. S. Tokuji, H. Awane, H. Yorimitsu, and A. Osuka, "Direct Arylation of meso-Formyl Porphyrin," *Chemistry* 19 (2013): 64.

42. Y. Kawamata, S. Tokuji, H. Yorimitsu, and A. Osuka, "Palladium-Catalyzed β-Selective Direct Arylation of Porphyrins," *Angewandte Chemie International Edition* 50 (2011): 8867.

43. H. Yorimitsu and A. Osuka, "Organometallic Approaches for Direct Modification of Peripheral C—H Bonds in Porphyrin Cores," *Asian Journal of Organic Chemistry* 2 (2013): 356.

44. Y. Mitamura, H. Yorimitsu, K. Oshima, and A. Osuka, "Straightforward Access to Aryl-Substituted Tetrathiafulvalenes by Palladium-Catalysed Direct C–H Arylation and Their Photophysical and Electrochemical Properties," *Chemical Science* 2 (2011): 2017.

45. H. Saito, K. Yamamoto, Y. Sumiya, et al., "Palladium-Catalyzed C—H Iodination of Arenes by Means of Sulfinyl Directing Groups," *Chemistry, an Asian Journal* 15 (2020): 2442.

46. Y. Segawa, T. Maekawa, and K. Itami, "Synthesis of Extended π-Systems through C–H Activation," *Angewandte Chemie International Edition* 54 (2015): 66.

47. J. Yamaguchi, A. D. Yamaguchi, and K. Itami, "C–H Bond Functionalization: Emerging Synthetic Tools for Natural Products and Pharmaceuticals," *Angewandte Chemie International Edition* 51 (2012): 8960.

48. F. Shibahara and T. Murai, "Direct Arylation Strategies in the Synthesis of π-Extended Monomers for Organic Polymeric Solar Cells," *Asian Journal of Organic Chemistry* 2 (2013): 624.

49. A. Nitti, R. Po, G. Bianchi, and D. Pasini, "Direct Arylation Strategies in the Synthesis of π-Extended Monomers for Organic Polymeric Solar Cells," *Molecules* 22 (2017): 21.

50. A. Nitti, M. Signorile, M. Boiocchi, G. Bianchi, R. Po, and D. Pasini, "Conjugated Thiophene-Fused Isatin Dyes through Intramolecular Direct Arylation," *The Journal of Organic Chemistry* 81 (2016): 11035.

51. A. Nitti, G. Bianchi, R. Po, T. M. Swager, and D. Pasini, "Domino Direct Arylation and Cross-Aldol for Rapid Construction of Extended Polycyclic π-Scaffolds," *Journal of the American Chemical Society* 139 (2017): 8788.

52. T. P. Osedach, T. L. Andrew, and V. Bulović, "Effect of Synthetic Accessibility on the Commercial Viability of Organic Photovoltaics," *Energy & Environmental Science* 6 (2013): 711.

Supporting Information

Additional supporting information can be found online in the Supporting Information section. **Supporting Fig. S1a:** The UV-Vis absorption and

photoluminescence spectra of **WKC04** and **WKC05** in CH_2Cl_2 solution. **Supporting Fig. S1b:** The UV-Vis absorption and photoluminescence spectra of **LHL01** and **LHL04** in CH_2Cl_2 solution. **Supporting Fig. S2a:** Cyclic voltammetry spectra of **WKC04** and **WKC05** in CH_2Cl_2 solution. **Supporting Fig. S2b:** Cyclic voltammetry spectra of **LHL01** and **LHL04** in CH_2Cl_2 solution. **Supporting Fig. S3a:** Thermogravimetric analysis curves of **WKC04** and **WKC05**. **Supporting Fig. S3b:** Thermogravimetric analysis curves of **LHL01** and **LHL04**. **Supporting Fig. S4:** J-V curves for the determination of the hole mobility of HTMs in the space-charge limited current (SCLC) region (HTMs spin-coated from PhCl). **Supporting Fig. S5:** Steady-state PL spectra of the devices fabricated as glass/perovskite/HTMs (HTMs spin-coated from PhCl). **Supporting Fig. S6:** Time-resolved PL spectra of the devices fabricated as glass/perovskite/HTMs (HTMs spin-coated from PhCl). **Supporting Fig. S7:** Mass Spectrum of **WKC04** (MALDI). **Supporting Fig. S8:** Mass Spectrum of **WKC05** (MALDI). **Supporting Fig. S9:** Mass Spectrum of LHL01 (MALDI). **Supporting Fig. S10:** Mass Spectrum of LHL04 (MALDI). **Supporting Fig. S11:** 1H NMR Spectrum of **WKC04** (500 MHz, THF-d8). **Supporting Fig. S12:** 13C NMR Spectrum of **WKC04** (125 MHz, THF-d8). **Supporting Fig. S13:** 1H NMR Spectrum of **WKC05** (500 MHz, THF-d8). **Supporting Fig. S14:** 13C NMR Spectrum of **WKC05** (125 MHz, THF-d8). **Supporting Fig. S15:** 1H NMR Spectrum of **LHL01** (500 MHz, $CDCl_3$). **Supporting Fig. S16:** 13C NMR Spectrum of LHL01 (75 MHz, $CDCl_3$). **Supporting Fig. S17:** 1H NMR Spectrum of **LHL04** (500 MHz, CD_2Cl_2).